Mar Geophys Res
DOI 10.1007/s11001-013-9190-8

Significant improvements in marine gravity from ongoing satellite missions

K. M. Marks • W. H. F. Smith • D. T. Sandwell

Received: 14 May 2013/ Accepted: 17 August 2013

Abstract Incorporating new altimeter data from CryoSat-2 (30 months), Envisat (18 months), and Jason-1 (7 months) satellites into an updated marine gravity field yields significant reduction in noise and improved resolution. Compared to an older gravity field that did not include the new altimeter data, incoherent power is reduced globally by approximately 2.9 dB at 15 km, 1.6 dB at 20 km, and 1.0 dB at 25 km wavelengths. Coherence analyses between the updated gravity and recent multibeam surveys distributed throughout the world's oceans shows an average increase of ~0.023 in mean coherence in the 20–160 km waveband, with the biggest increase (>0.08) over fast spreading ridges and smallest (<0.02) over slow spreading ridges and continental shelves. The shortest wavelength at which coherence is above 0.5 decreased globally by ~2 km wavelength, with the biggest decrease (>3.5 km) over fast spreading ridges and smallest (<1.5 km) over slow spreading ridges and continental shelves. In the Clipperton fracture zone area these improvements result in seamounts that are more accurately located, the detection of smaller seamounts, and the expression of north-south trending abyssal hill fabric. As more altimeter data from the ongoing satellite missions are incorporated into future gravity field updates, finer-scale details of the seafloor will continue to emerge.

K. M. Marks (✉) · W. H. F. Smith
NOAA Laboratory for Satellite Altimetry, E/RA 31, 5830 University Research Court, College Park, MD 20740, USA
e-mail: karen.marks@noaa.gov

D. T. Sandwell
Scripps Institution of Oceanography, La Jolla, CA 92093, USA

Published online: 30 August 2013

Keywords Satellite gravity · Multibeam · Bathymetry · Coherence · Noise

Introduction

The marine gravity field has been effectively mapped using altimeter data from Geosat and ERS-1 satellites (Sandwell and Smith 1997). The close satellite track spacing (~6 to 8 km at the equator) from these missions' geodetic phases combined with high precision from repeat tracks enabled the derivation of gravity anomalies of unprecedented resolution over the world's oceans. The marine gravity anomalies were subsequently used to estimate depths in poorly surveyed areas, and combined with ship soundings, the global seafloor was mapped in detail for the first time (Smith and Sandwell 1997).

Between 1995 and 2010 there were no new altimeter data collected along densely-spaced tracks. Improvements to the marine gravity field were made by retracking the old ERS-1 (Sandwell and Smith 2005) and Geosat (Sandwell and Smith 2009) geodetic mission data. In the last few years, the CryoSat-2 and Jason-1 missions have collected data in geodetic phases that, when incorporated into the gravity model, serve to augment existing satellite track coverage and therefore increase the data density. Envisat also flew some new tracks for a short time (18 months) before its demise. Data from these altimeters are also more precise than data from Geosat and ERS-1, because the pulse repetition frequency of these satellites is about twice that of Geosat and ERS-1, doubling the data averaging available per second of flight of the spacecraft (Garcia et al. 2013).

To assess the resulting gravity field improvements, we compared a gravity field that incorporated these recent satellite data (version 21) to a field that did not (version 18). Both versions were produced by Sandwell and Smith following their published methods (Sandwell

and Smith 1997, 2009; Sandwell et al. 2013). We employ a technique that compares the gravity field estimate to regional multibeam surveys that serve as topography "ground truth" (Marks and Smith 2012). Cross-spectral coherency between these two inputs measures the linear correlation between them as a function of wavelength. Higher coherence between gravity and bathymetry anomalies to shorter wavelengths, along with reductions in noise, are indicative of improvements. This approach is conservative, because only that portion of the gravity anomaly field that can be produced by a linear filter operating on bathymetry is considered "coherent," or "signal;" all other aspects of the gravity input, including not only error but also true signals from sub-seafloor and non-linear seafloor components, are considered "noise." Thus we over-estimate the noise amplitude and we under-estimate the true signal to true noise ratio. Details follow later.

We used this technique in our recent coherence analysis between gravity version 18 and regional multibeam surveys located throughout the world's oceans (Marks and Smith 2012). This study found that the mean coherence averaged over the 20-160 km waveband, and the shortest wavelength at which coherence is above 0.5, varies with tectonic setting. In the research presented here, we revisit this analysis but with gravity version 21 that incorporates additional CryoSat-2 (30 months), Envisat (18 months), and Jason-1 (7 months) geodetic phase data. More importantly, we exploit the new coherence analysis results to measure the reduction in "noise" (by the definition above) that the additional altimeter data, precision, and retracking afford. We find that the most significant improvements are in areas where the tectonic fabric of the seafloor has low amplitude, such as at fast-spreading ridges, and we illustrate the improvements at the East Pacific rise near the Clipperton fracture zone.

Data

In this study we used the same twenty-five regional multibeam surveys that were used in Marks and Smith (2012), and we use a new, updated gravity field. The multibeam grids were downloaded from the National Geophysical Data Center, the University of New Hampshire, Lamont-Doherty Earth Observatory, Geoscience Australia, and the University of Hawaii. The locations of the multibeam grids are shown in Fig. 1. Corresponding satellite-derived gridded gravity data (version 21) are an update of Sandwell and Smith (2009; Sandwell et al. 2013). The gravity grid is on a Mercator projection with 1-minute grid spacing while the twenty-five multibeam grids came in a variety of projections and grid spacings.

Details of grid preparation are described in Marks and Smith (2012), but a brief summary here is that (1) multibeam surveys having adequate map extent, coverage, and grid spacing were selected, (2) the gravity grid was sampled at each multibeam grid point and then both the gravity and bathymetry were projected with an Oblique Mercator projection to maximize the rectangular extent of the coverage for each area, (3) the projected points were interpolated onto regular grids with 1000 m spacing, and (4) square subsets completely filled with data were extracted. This preparation yielded gravity and bathymetry grids ready for analysis using two-dimensional Fourier transform cross-spectral techniques.

Coherence and noise analysis

It is appropriate to use radially symmetric coherence analysis on gravity and bathymetry grids because all anomalies in two dimensions are taken into account (Marks and Smith 2012). This is in contrast to one-dimensional coherence along ship tracks, where the gravity anomaly profile includes the effect of topography off to the side of the track, which can bias the coherence estimates to a lower value.

The coherence between a pair of inputs is the square of the linear correlation coefficient as a function of wavelength, indicating how much of the variance in one input can be correlated with the other through a linear filtering operation. Coherence near 1 indicates nearly perfect linear correlation, while coherence near 0 indicates the absence of any significant linear relationship. A coherence of 0.5 can be interpreted as a signal-to-noise ratio of 1:1 if one input can be assumed to be noise-free (Bendat and Piersol 1986, Eq. 6.39).

The equation for radially symmetric coherence estimation is:

$$\text{Coherence} = | \langle GB^* \rangle |^2 / (\langle GG^* \rangle \langle BB^* \rangle) \qquad (1)$$

where G and B are obtained from the Fourier transformation of the gravity and bathymetry grids, * is the complex conjugate, and brackets $< >$ represent averaging azimuthally within radial wavebands.

We used GMT (Wessel and Smith 1998) routine "gravfft" (J. Luis, personal communication, 2011) to compute radially symmetric coherence. This routine, a generalization of GMT routine "grdfft," applies the Fast Fourier Transform to the input grids, performs the coherence operation, and outputs the coherence averaged azimuthally as a function of wavelength. Details are in Marks and Smith (2012).

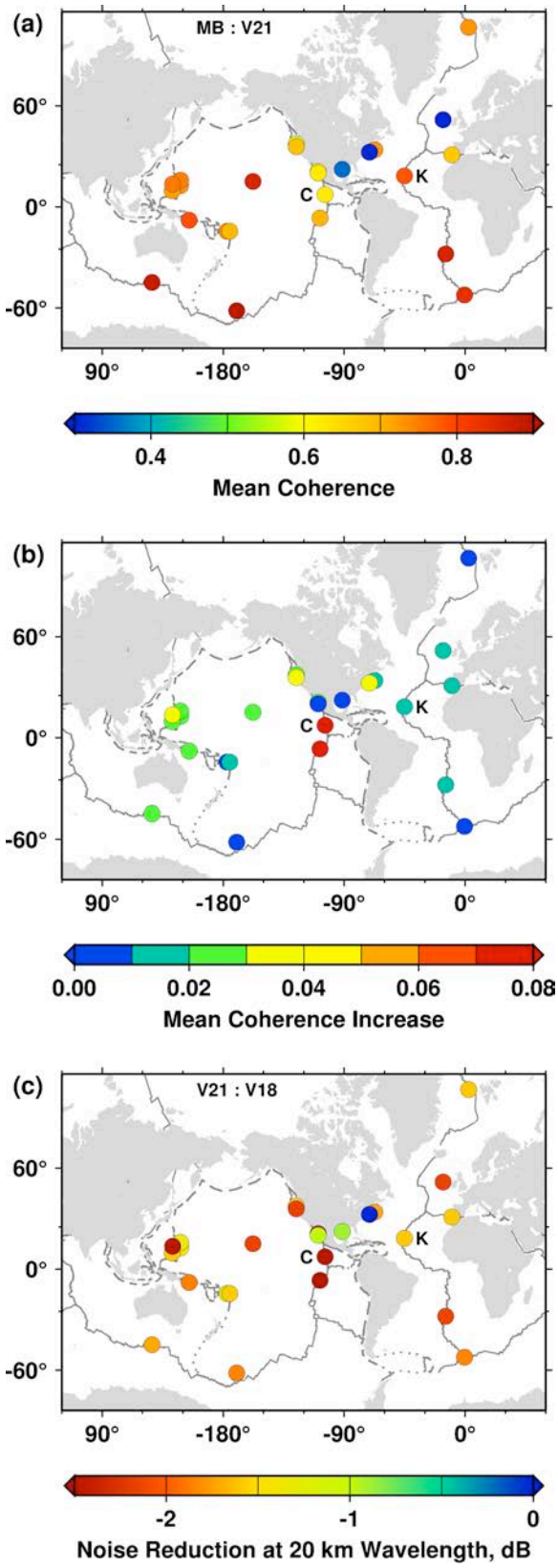

◀ **Fig. 1** Twenty-five areas analyzed in this study. *Colors* indicate **a** mean coherence between satellite-derived gravity V21 and multibeam depths over the 20-160 km waveband, **b** increase in mean coherence between V21 and V18 over the 20-160 km waveband, and **c** noise reduction between V21 and V18 at 20 km wavelength; larger reductions are more negative, zero is no reduction. Tectonic settings are spreading ridges (*solid lines*), trenches (*dashed lines*), continental shelves (offshore California, New England, Gulf of Mexico, Spain, Ireland), seamounts (Hawaii and offshore New England), and transform plate boundaries (*dotted lines*). Clipperton (*C*) and Kane (*K*) fracture zone areas are notated

The coherence results can be used to find the ratio between noise power in the new version 21 and the older version 18 gravity fields. The squared coherency, C, is a function of signal S and noise N power:

$$C = S/(S+N) \tag{2}$$

Rearranging gives the ratio of noise-to-signal:

$$N/S = (1/C) - 1 \tag{3}$$

Taking the ratio of noise-to-signal for both versions 21 and 18 gives:

$$(N_{V21}/S_{V21}) / (N_{V18}/S_{V18}) \tag{4}$$

Because the signal power must be the same in both gravity versions, it can be canceled out, leaving the ratio of the noise power in version 21 to the noise power in version 18:

$$N_{V21}/N_{V18} = \{(1/C_{V21}) - 1\} / \{(1/C_{V18}) - 1\} \tag{5}$$

However in the context of coherency with bathymetry, gravity "signal" and "noise" are not the same as "truth" and "error" in the gravity field. It may be helpful to imagine that any version of the satellite-derived gravity field is composed of three parts:

$$Grav_{V\#} = Corr\_g + (OTG + E_{V\#}) \tag{6}$$

Corr_g is that portion of the total gravity field that is "coherent" with the seafloor topography, in the sense that coherency is used in this paper. This means it is the portion of the gravity field that can be correlated with the seafloor topography through a linear, spatially invariant, and radially symmetric operator. If the seafloor topography represents an interface between two volumes each having a constant density, then the first-order approximation for the gravity anomaly at the sea surface due to topography on the seafloor (Parker 1973) would be such an operator. If the isostatic compensation of the seafloor topography is determined by a linear, spatially invariant and radially symmetric operation then this isostatic compensation also, to first

order, would be included in *Corr_g*. Airy, Pratt, and flexural isostasy (Watts 2001) are of this kind.

The coherency analysis employed here identifies the *Corr_g* component as signal and treats everything else as "noise." This "noise" is the sum of two components. One is labeled *OTG*, for "other true gravity," in Eq. 6. *OTG* is that gravity anomaly field that truly exists in Earth's gravity field, but which is not coherent with the seafloor topography by our definition of coherence. *OTG* arises from heterogeneities in density and sub-seafloor structure not associated with seafloor topography or its isostatic compensation, and also from higher-order non-linear terms in the gravitational attraction of the seafloor and its compensation. The second component of "noise" is error in the data comprising a gravity field model, labeled *E* in Eq. 6. Since each version of a model may have its own sources of error, the field model and its *E* are given a subscripted version number.

It is important to understand that we cannot separate the three components individually. What one would like to know is the nature of the error term, *E*, and its size relative to the total true gravity, *Corr_g* + *OTC*. But we cannot determine this. If we form the difference $Grav_{V21} - Grav_{V18}$ the total gravity cancels, leaving $E_{V21} - E_{V18}$. By definition this is incoherent with the bathymetry, and is thus all "noise" in our analysis. However, the error difference also cancels any errors that are common to both versions. If there are no common errors then the spectrum of the differenced fields contains the sum of the power in each error field separately, and hence over-estimates the error in any one version, while if there are common errors, these are not counted and so are under-estimated. Therefore we cannot determine the magnitude of *E* by this means.

Comparing the coherency determined from two versions can give us a noise power ratio, N_{V21}/N_{V18}, (Eq. 5) but this ratio is in fact $(OTG + E_{V21})^2 / (OTG+E_{V18})^2$, not $(E_{V21})^2/(E_{V18})^2$ (coherency compares coherent and incoherent power, or variance, not standard deviations). If the standard deviation of E_{V21} is 1 mGal and the standard deviation of E_{V18} is 2 mGal while the root-mean-square amplitude of *OTG* is 5 mGal, then $(E_{V21})^2/(E_{V18})^2 = ¼$, while $N_{V21}/N_{V18} = 26/29$. Here we have assumed that *OTG* and *E* are uncorrelated, so that $(OTG + E)^2 = OTG^2 + E^2$ in a power spectral sense. Thus if there is any *OTG* at all then the "noise" reduction determined here must under-estimate the error reduction in the models. We note that because modern multibeam bathymetry measurements are accurate to a few tenths of a percent of depth (Marks and Smith 2009), bathymetry may be considered to be noise-free for our analysis.

Results

Global

In Fig. 1a we show the results of coherence analysis between gravity version 21 and multibeam bathymetry for all twenty-five study areas. The mean coherence is calculated over the 20–160 km waveband because gravity and topography may be correlated at these wavelengths (Smith and Sandwell 1994). At shorter wavelengths, gravity anomalies are attenuated by upward continuation from the seafloor to the sea surface, and longer wavelengths are mostly canceled out by isostatic compensation. Compared to our previous analysis using gravity version 18 (Marks and Smith 2012; Fig. 1), the mean coherence has increased overall by ~0.023 using gravity version 21. It increased most (>0.08) over fast spreading ridges that have relatively smooth topography (MacDonald 1982) and subdued gravity anomalies (Jonas et al. 1991), and least (<0.02) over slow spreading ridges that have rough topography with highly correlated gravity anomalies, and over continental shelves (Fig. 1b). Where coherence was already high it increased less, and where it was only moderate, it increased more. Consistent with our previous research, the mean coherence varies as a function of tectonic setting: seamounts and slow spreading ridges have high (>0.7) mean coherence, other spreading ridges and trenches have intermediate (0.5-0.7) coherence, and continental shelves have low (<0.5) coherence.

Improvements in resolution can be estimated by the shortest wavelength at which coherence is above 0.5. On average, the shortest wavelength decreased by ~2 km, with the biggest decrease (>3.5 km) over fast spreading ridges and the smallest (<1.5 km) over slow spreading ridges and continental shelves. Note here that "resolution" means in the sense of signal and noise as these terms are used in this paper, meaning not "above true noise" but rather "predictable when bathymetry is predicted from gravity."

We used the coherence results to calculate the ratios of noise power in gravity version 21 to noise power in version 18, via Eq. 5 in the previous section. These ratios are plotted in Fig. 2. When the noise power is lower in version 21 than in version 18, the ratio (in decibels) is negative. Fig. 2 shows that noise is reduced in gravity version 21, and that the reduction increases as wavelength decreases.

Coherence is increased at shorter wavelengths as a result of the additional satellite data that was incorporated into gravity version 21, and the increased precision. In particular, new ground tracks from Jason-1 and CryoSat-2 are filling in the space between Geosat and ERS-1 ground tracks, increasing the data density so that the effective track spacing is closer to 4 km at the equator. Further, Jason-1 has a lower orbit inclination

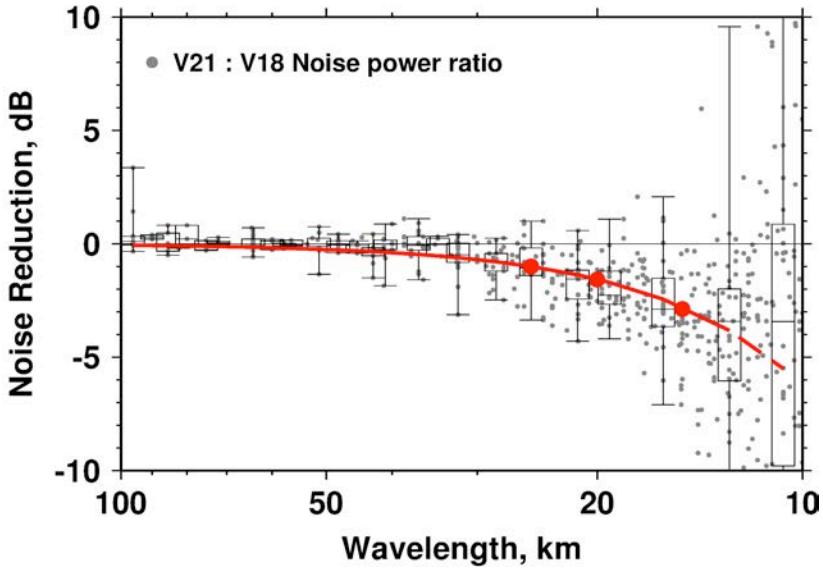

Fig. 2 Noise reduction as a function of wavelength. *Gray dots* are the ratio of noise power between satellite-derived gravity V21 and V18 for twenty-five areas distributed throughout the world's oceans (see Fig. 1); *red line* fits ratio medians and *box bottoms* and *tops* are the 25% and 75% quantiles, respectively. Noise is reduced by approximately 2.9 dB at 15 km, 1.6 dB at 20 km, and 1.0 dB at 25 km wavelengths (*red circles*)

resulting in a more east-west orientation of its ground tracks. Longer wavelength (>50 km) anomalies are already well resolved by the ~6 to 8 km ground track spacing of gravity version 18 so the increased data density of version 21 does not increase the coherence much at these wavelengths.

Fig. 1c shows in map view the amount of "noise" (incoherent power) reduction at 20 km wavelength for all the study areas. Noise is reduced most over fast and medium rate spreading ridges and seamounts, and least over continental shelves. Small gravity signals, arising from relatively smooth topography typical of fast (and medium) rate spreading ridges, become more prominent as noise is reduced. Large gravity anomalies correlated with the rough topography of slow spreading ridges, on the other hand, already predominate over the noise. Over continental shelves, gravity anomalies arising from sub-seafloor density structures are uncorrelated with the flat topography.

Clipperton fracture zone area

The Clipperton fracture zone area (located in Fig. 1) demonstrates our results. Multibeam data covering the Clipperton fracture zone and a segment of the fast-spreading East Pacific rise to the south are shown in Fig. 3a. Fine-scale details of the seafloor such as seamounts, abyssal hills, the spreading ridge axis, and fracture zones are evident. Corresponding satellite-derived gravity anomaly grids are shown in Fig. 3c, d.

Radially symmetric coherence between the gravity version 21 (or 18) grid and the multibeam grid is shown in Fig. 4a. The results show coherence > 0.5 for wavelengths greater than 21 km for gravity version 21, and for wavelengths greater than 26 km for gravity version 18. The higher coherence to shorter wavelengths in gravity version 21 indicates a significant improvement in fine-scale resolution. Indeed, the improvement can be observed in Fig. 3d (compared to Fig. 3c) as enhanced north-south trending abyssal hill fabric and the visualization of smaller seamounts.

We also calculated the ratio of noise power in gravity versions 21 and 18 (Fig. 4b). Consistent with the global results, noise is reduced in gravity version 21, and the reduction increases with decreasing wavelength. However in this study area the noise power ratio begins to turn upwards so that there is less noise reduction over wavelengths shorter than 16 km. This is because there are very short wavelength topography anomalies that are not in the gravity due to upward continuation- these anomalies are very low amplitude at fast-spreading ridges, and hence the coherency analysis finds no signal power at these wavelengths.

In Fig. 4c we compare the power spectral densities of the Clipperton fracture zone area on the fast-spreading East Pacific rise to the Kane fracture zone area on the slow-spreading Mid-Atlantic ridge (located in Fig. 1). Gravity version 21 has significantly more power at wavelengths longer than about 13 km in the Kane fracture zone area than in the Clipperton area. This is because the large amplitude gravity anomalies arising from the rough topography of slow-spreading ridges contain more power than the subdued, low amplitude gravity anomalies arising from the smooth seafloor of fast-spreading ridges. The power spectral densities of the differences obtained by subtracting gravity version 18 from version 21 in each area are also plotted in Fig. 4c. There is more power in the differences in the Clipperton fracture zone area than in the Kane area. Further, the ratio of difference-to-signal variance in the Clipperton area is about 14 %, and in the Kane area it is less than 1 %. Although signals in the Clipperton area are smaller than in the Kane area, relative to the difference level, they are larger. This

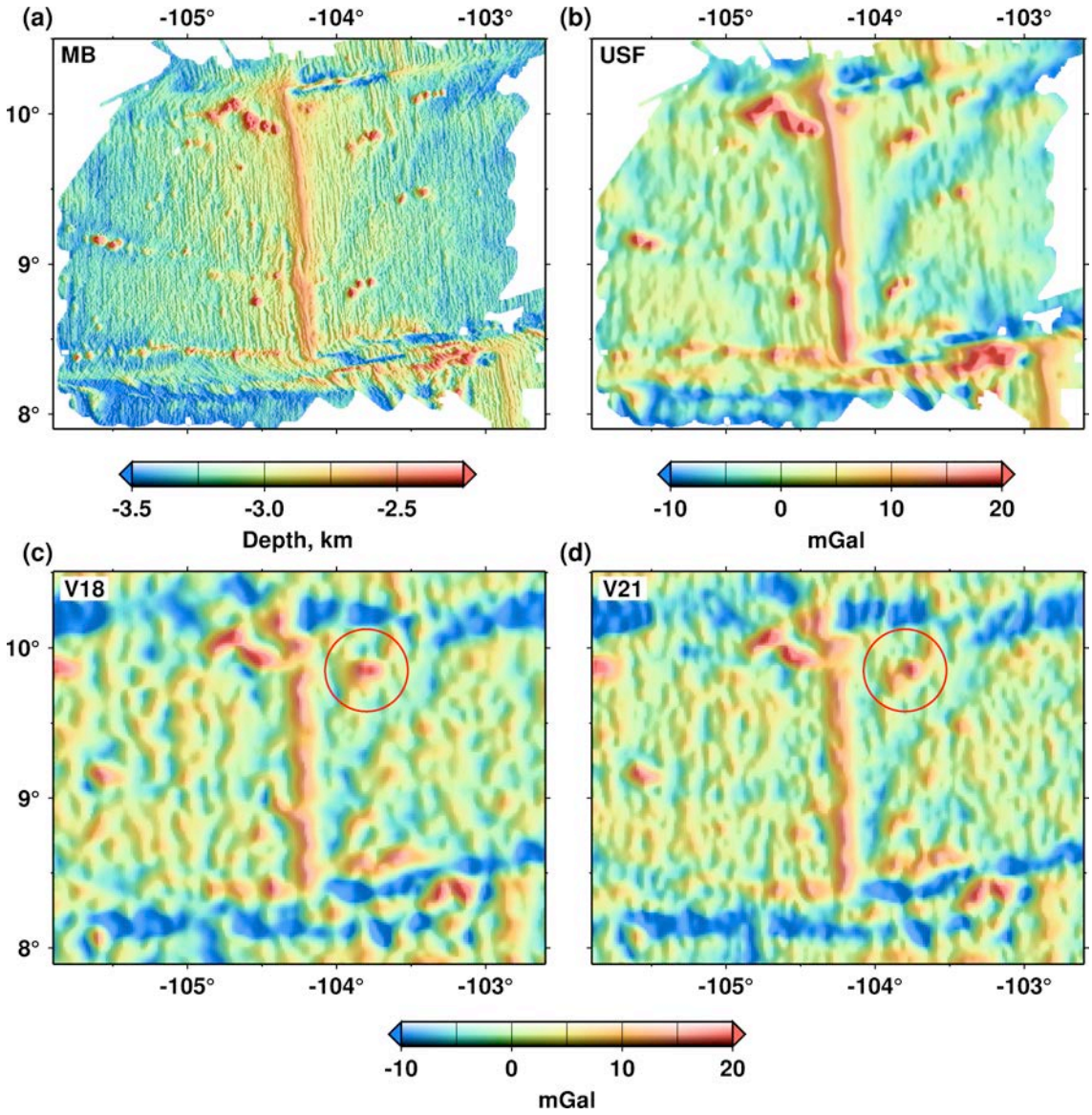

Fig. 3 **a** Regional multibeam bathymetry, **b** upward-continued seafloor (USF) calculated from **(a)**, satellite-derived gravity **c** V18 and **d** V21, over the Clipperton fracture zone area. Planar trends were removed from grids shown. *Circles* encompass seamounts as resolved in **c** V18 and **d** V21

explains our finding that noise is reduced most over fast (and medium) rate spreading ridges.

Also plotted in Fig. 4c are power spectral densities for the portion of gravity that is correlated with topography (coherent power), and the portion that is not correlated (incoherent power). It is these spectral densities that are the "signal" and "noise" power in our derivation of Eq. 5. In the Clipperton area, the wavelength at which the power spectral density of uncorrelated gravity is as large as that of correlated gravity (~21 km) is the same as the wavelength at which gravity version 21 coherence crosses 0.5 in Fig. 4a. This is approximately the shortest wavelength at which bathymetry can be predicted from gravity with confidence. The power spectral density of the differences between version 21 and 18 is as large as that of version 21 at ~12 km wavelength. If the differences between versions 21 and 18 can be taken as a proxy for the uncertainty in the field (i.e., the true "error"), then the wavelength where true signal equals true error is ~12 km. Upward continuation may account for the difference between 21 and 12 km wavelength. This illustrates that incoherence is not due to true error alone, and gives a pessimistic estimate of spatial resolution.

In Fig. 3b we seek to display the "best case" gravity anomalies that could be detected at the sea surface if gravity observations were extremely dense, there were no measurement errors, and there were no signal from

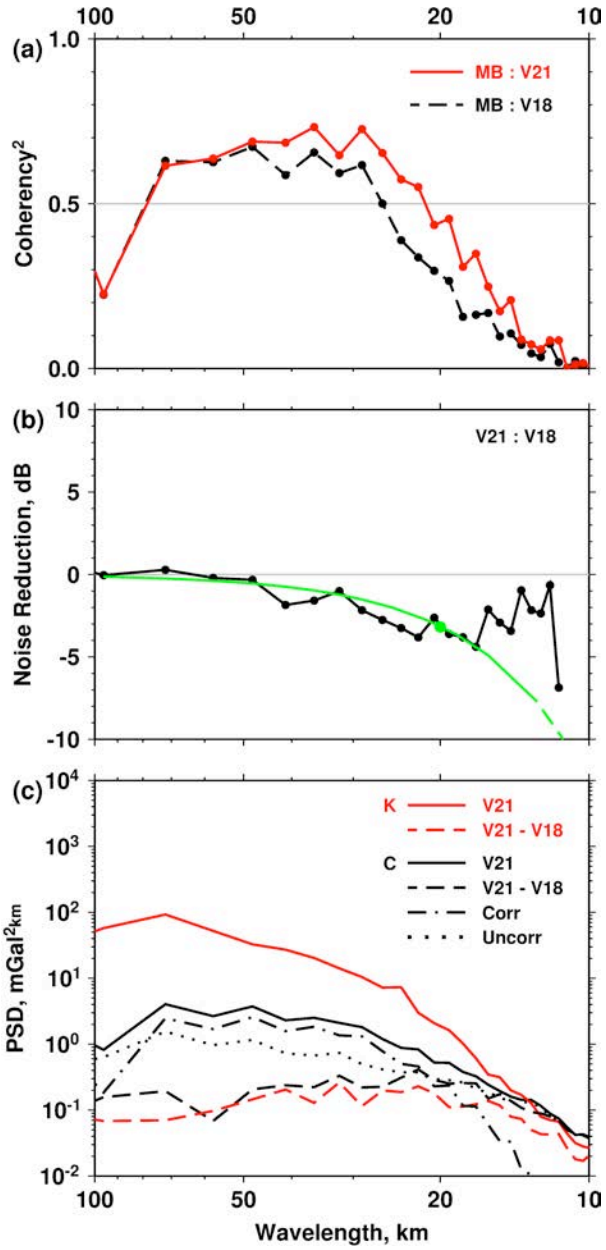

Fig. 4 **a** Radially symmetric coherence between satellite-derived gravity V21 (*red line*) or V18 (*black line*) and multibeam grids (shown in Fig. 3) over the Clipperton fracture zone area (notated in Fig. 1). **b** Ratio of noise power between V21 and V18 is reduced by 3.2 dB at 20 km wavelength (*green circle*). *Green curve* fits noise power ratio. **c** Power spectral densities (PSD) of Kane gravity V21 (*solid red line*) and V21 – V18 differences (*dashed red line*), and of Clipperton gravity V21 (*solid black line*), V21 – V18 differences (*dashed black line*), gravity correlated with bathymetry (Corr) (*dash-dot black line*), and gravity uncorrelated with bathymetry (Uncorr) (*dotted black line*). K and C are notated in Fig. 1

sub-seafloor sources. We calculated these gravity anomalies from the multibeam depths in Fig. 3a by multiplying by a scaling factor, upward continuing from the seafloor to the sea surface, and filtering to pass wavelengths < 160 km. This procedure approximates the gravity signal that may be correlated with the underlying seafloor topography (Smith and Sandwell 1994). Notably the north-south trending abyssal hill fabric is evident as are very small seamounts. There is more of a resemblance to gravity version 21 (Fig. 3d) than 18 (Fig. 3c).

A pair of adjacent seamounts located at -103.8° W, 9.85° N are well resolved in the multibeam survey (Fig. 3a) and in the upward-continued seafloor anomalies (Fig. 3b). However the gravity high associated with the westernmost seamount peak lies due west of the adjacent one in gravity version 18 (circled in Fig. 3c). In version 21, the gravity high from the westernmost peak lies southwest of the adjacent one (circled in Fig. 3d), which matches the configuration observed in the multibeam and upward-continued seafloor anomalies.

Profiles along ship tracks in the Clipperton fracture zone area are plotted in Fig. 5. These tracks were selected to examine signals from small seamounts and also from abyssal hills. Ship surveys MW8706 (B-B') and MW8707 (C-C') were collected by R/V *Thomas Washington* in 1987, and survey RAIT01 (A-A') was collected by R/V *Moana Wave* in 1988.

Two small (~7 km wide, ~1 km tall) adjacent seamounts are present in MW8706 ship bathymetry and multibeam (B-B'). The ship gravity and upward-continued seafloor anomalies both show highs over each seamount peak. However gravity versions 18 and 21 both show only a single gravity anomaly high covering both seamount peaks. A larger (~13 km wide, ~1 km tall) seamount is present in MW8707 ship bathymetry and multibeam. The ship gravity, upward-continued seafloor, and gravity version 18 and 21 anomalies all show highs correlated with the seamount.

We attempt to estimate the typical width of a bathymetric feature such as a seamount that can be predicted from gravity with a linear filter. Coherency (Eq. 1) may be interpreted as the spectral transfer function of a Wiener filter that should be applied to the gravity to minimize the mean square error in the estimated bathymetry (Press et al. 1986, Eq. 12.6.6; Smith and Sandwell 1994, Appendix). Since the coherency is radially symmetric, the impulse response of this filter is the Hankel transform of the coherency. We computed this Hankel transform and measured the diameter of the impulse response at half its maximum, obtaining 11 km. This diameter is an estimate of the typical width of a bathymetric feature that can be predicted from bathymetry with confidence. However, because it is estimated from coherency with bathymetry, it is not the scale at which the true gravity rises above the gravity error. That scale would be shorter, and cannot be determined from the coherency used here. The two small seamounts in profile MW8706 have widths smaller (<11 km) than can be predicted from gravity with confidence.

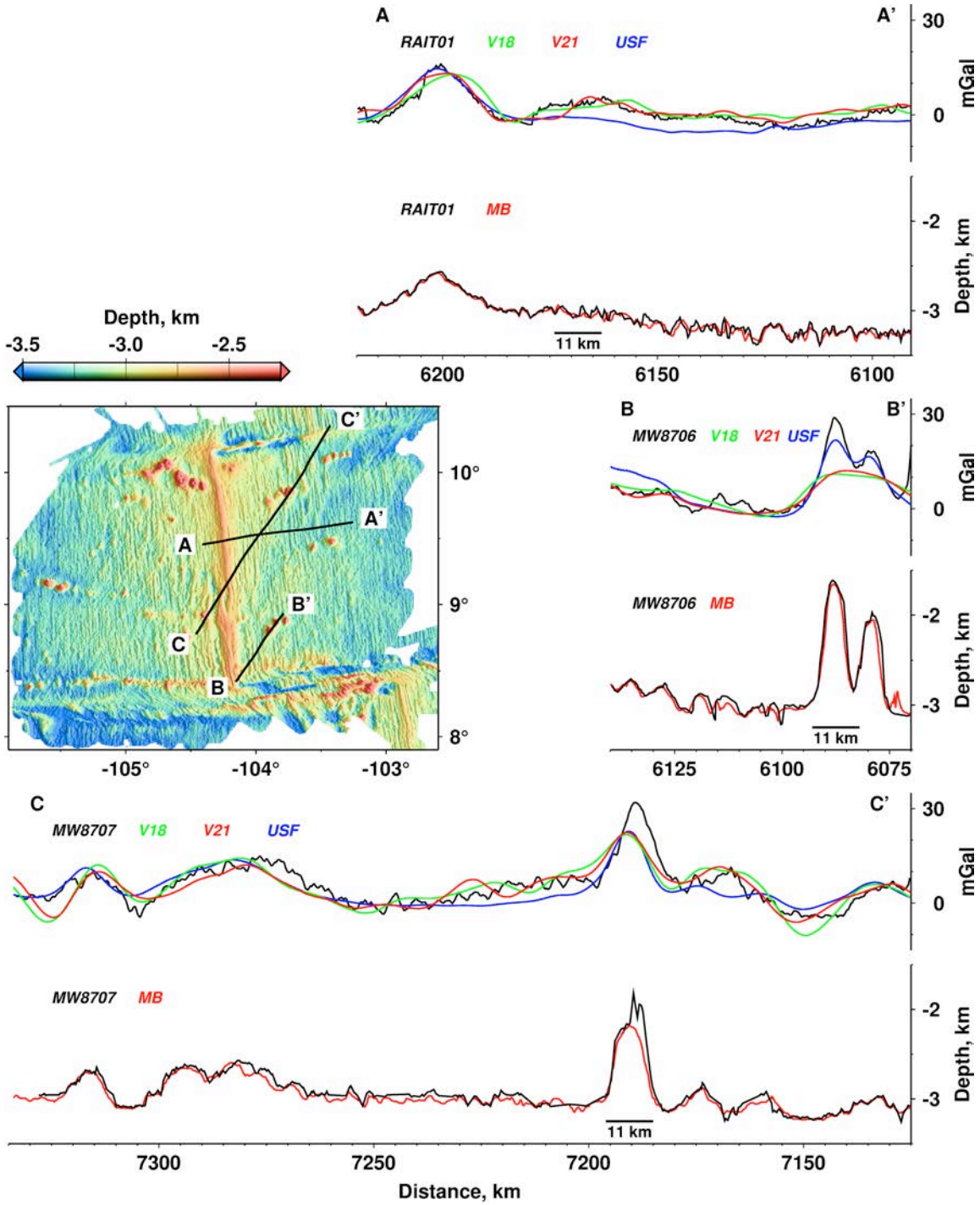

Fig. 5 Gravity and bathymetry profiles plotted along ship survey tracks crossing the East Pacific rise, abyssal hills, and small seamounts in the Clipperton fracture zone area. Seafloor features wider than ~11 km may be resolved in satellite-derived gravity. USF defined in Fig. 3 caption.

Abyssal hills are abundant on the flanks of the East Pacific rise (Fig. 5). They are narrow, low-relief (2-5 km wide, 50-300 m high) horsts and grabens (Macdonald et al. 1996) that are tens of kilometers long in the north-south direction. Therefore in this study area signals from abyssal hills are anisotropic- very short wavelength in the east-west direction and long wavelength in the north-south direction. All three ship surveys cross the abyssal hill fabric so that mostly the abyssal hill widths would be observed in the profiles (especially profile RAIT01). Very short wavelength bumps are observed in the topography, but the

corresponding upward-continued seafloor anomalies and satellite-derived gravity profiles are smooth. Gravity signals from these topographic bumps are attenuated by upward continuation, accounting for the smooth corresponding gravity profiles. In contrast, the north-south trending abyssal hill signal is of sufficiently long wavelength to be detected in the upward-continued seafloor anomaly grid (Fig. 3b) and is suggested in the gravity version 21 grid (Fig. 3d).

Goff et al. (2004) studied the possibility of detecting gravity anomalies oriented along the long axis of abyssal hills in the presence of gravity field errors. They created synthetic seafloor topography models with random fractal textures appropriate for abyssal hills on slow, intermediate, and fast spreading ridges, computed the gravity attraction of these textures upward continued to the sea surface, added white noise to these gravity models, and then searched for discernable fabric orientation in the resulting field. For fast spreading ridges such as in the Clipperton fracture zone area, they found the strike of the gravity fabric partially resolved in a white noise level of 1 mGal, but undetectable in a white noise level of 4 mGal. In contrast, the stronger anomalies at slow spreading ridges such as in the Kane fracture zone area showed detectable fabric even if the white noise level reached 4 mGal. We can see the orientation of the abyssal hill fabric in gravity version 21 (Fig. 3d) but not in version 18 (Fig. 3c). If the results of Goff et al. obtained from synthetic models with purely white errors can be applied to the actual data shown here, then a true error level approaching 1 mGal in version 21 is suggested. A comparison between gravity version 21 and ship gravity in the Gulf of Mexico (Sandwell et al. 2013) finds an error level of 1.7 mGal in agreement with our estimate.

Concluding remarks

We have shown that incorporating additional CryoSat-2, Envisat, and Jason-1 (just 7 months) satellite data into gravity version 21 has led to a significant reduction in noise and increased resolution. These improvements result from 1) ground tracks that fill in the spaces between Geosat and ERS-1 tracks and hence increase data density, 2) the lower orbital inclination of Jason-1 that enhances east-west component resolution, and 3) increased precision due to additional repeat tracks and the higher pulse repetition rate of the newer satellites.

We assessed these improvements using coherence and noise analysis techniques. Globally, there is an overall increase in mean coherence in the 20-160 km waveband where gravity and bathymetry anomalies may be correlated, and there is a decrease in the shortest wavelength at which coherence is above 0.5. Also globally, noise is reduced in the updated satellite-derived gravity, with the reduction growing larger with decreasing wavelength. Notably noise is reduced most over tectonic settings having relatively smooth seafloor and subdued gravity anomalies- in these areas small signals emerge when the noise level is lowered.

The impact of these global improvements is demonstrated in the Clipperton fracture zone area. Gravity version 21 incorporating the new satellite data reveals a north-south trending fabric that may arise from numerous abyssal hills, and seamounts are more accurately located. In this study area, “noise” (incoherent power) was reduced by 3.2 dB at 20 km wavelength, and anomalies down to 21 km in wavelength are resolved.

As data from ongoing satellite missions continues to be incorporated into gravity field updates, even finer-scale features of the seafloor- including small seamounts- may become more evident and more accurately mapped. Better bathymetric predictions (Smith and Sandwell 1997) will follow using the updated marine gravity fields that incorporate the additional satellite data.

Acknowledgements The comments of an anonymous reviewer improved this manuscript. GMT software (Wessel and Smith 1998) was used to make figures and perform computations. The views, opinions, and findings contained in this report are those of the authors and should not be construed as an official National Oceanic and Atmospheric Administration or U.S. Government position, policy, or decision.

This article is available online at:
http://link.springer.com/article/10.1007/s11001-013-9190-8

References

Bendat JS, Piersol AG (1986) Random data: analysis and measurement procedures, 2nd edn. Wiley, New York

Garcia ES, Smith WHF, Sandwell DT, (2013) Retracking CryoSat-2, Envisat, and Jason-1 radar altimetry waveforms for improved gravity field recovery. Geophys J Int, under revision

Goff JA, Smith WHF, Marks KM (2004) The contributions of abyssal hill morphology and noise to altimetry gravity fabric. Oceanography 17:24-37

Jonas J, Hall S, Casey JF (1991) Gravity anomalies over extinct spreading centers: a test of gravity models of active centers. J Geophys Res 96:11,759-11,777. doi:10.1029/91JB-00617

Macdonald KC (1982) Mid-ocean ridges: fine scale tectonic, volcanic and hydrothermal processes within the plate boundary zone. Ann Rev Earth Planet Sci 10:155-190. doi:10.1146/annurev.ea.10.050182.001103

Macdonald KC, Fox PJ, Alexander RT, Pockalny R, Gente P (1996) Volcanic growth faults and the origin of Pacific abyssal hills. Nature 380:125-129. doi:10.1038/380125a0

Marks KM, Smith WHF (2009) An uncertainty model for deep ocean single beam and multibeam echo sounder data. Mar Geophys Res 29:239-250. doi:10.1007/s11001-008-9060-7

Marks KM, Smith WHF (2012) Radially symmetric coherence between satellite gravity and multibeam bathymetry grids. Mar Geophys Res 33:223-227. doi:10.1007/s11001-012-9157-1

Parker RL (1973) The rapid calculation of potential anomalies. Geophys J Roy Astron Soc 31:447-455. doi:10.1111/j.1365-246X.1973.tb06513.x

Press WH, Flannery BP, Teukolsky SA, Vetterling WT (1986) Numerical recipes: the art of scientific computing. Cambridge University Press, Cambridge

Sandwell DT, Smith WHF (1997) Marine gravity anomaly from Geosat and ERS 1 satellite altimetry. J Geophys Res 102:10039-10054. doi:10.1029/96JB03223

Sandwell DT, Smith WHF (2005) Retracking ERS-1 altimeter waveforms for optimal gravity field recovery. Geophys J int 163:79-89. doi:10.1111/j.1365-246X.2005.02724.x

Sandwell DT, Smith WHF (2009) Global marine gravity from retracked Geosat and ERS-1 altimetry: ridge segmentation versus spreading rate. J Geophys Res 114:B01411. doi:10.1029/2008JB006008

Sandwell DT, Garcia ES, Soofi K, Wessel P, Smith WHF, (2013) Towards 1 mGal global marine gravity from CryoSat-2, Envisat, and Jason-1, Lead Edge, 32:892-899. doi:10.1190/tle32080892.1

Smith, WHF, Sandwell DT (1994) Bathymetric prediction from dense satellite altimetry and sparse shipboard bathymetry, J Geophys Res 99(B11):21803-21824. Doi:10.1029/94JB009988

Smith WHF, Sandwell DT (1997) Global sea floor topography from satellite altimetry and ship depth soundings. Science 277:1956-1962. doi:10.1126/science.277.5334.1956

Watts AB (2001) Isostasy and flexure of the lithosphere, Cambridge University Press, Cambridge

Wessel P, Smith WHF (1998) New, improved version of generic mapping tools released. EOS Trans AGU 79:579. doi:10.1029/98EO0042